Title

Investigation of coupling mechanisms in attosecond transient absorption of autoionizing states: comparison of theory and experiment in xenon

Authors

Li, Xuan
Bernhardt, Birgitta
Beck, Annelise R
et al.

Investigation of coupling mechanisms in attosecond transient absorption of autoionizing states: comparison of theory and experiment in xenon

Xuan Li[1], Birgitta Bernhardt[1,2], Annelise R Beck[1,2], Erika R Warrick[1,2], Adrian N Pfeiffer[1,2], M Justine Bell[1,2], Daniel J Haxton[1], C William McCurdy[1,3], Daniel M Neumark[1,2] and Stephen R Leone[1,2,4]

[1] Ultrafast X-ray Science Laboratory, Chemical Sciences Division, Lawrence Berkeley National Laboratory, Berkeley, California 94720, USA
[2] Department of Chemistry, University of California, Berkeley, California 94720, USA
[3] Department of Chemistry, University of California, Davis, California 95616, USA
[4] Department of Physics, University of California, Berkeley, California 94720, USA

E-mail: XuanLi@lbl.gov

CrossMark

Abstract
Attosecond transient absorption spectra near the energies of autoionizing states are analyzed in terms of the photon coupling mechanisms to other states. In a recent experiment, the autoionization lifetimes of highly excited states of xenon were determined and compared to a simple expression based on a model of how quantum coherence determines the decay of a metastable state in the transient absorption spectrum. Here it is shown that this procedure for extracting lifetimes is more general and can be used in cases involving either resonant or nonresonant coupling of the attosecond-probed autoionizing state to either continua or discrete states by a time-delayed near infrared (NIR) pulse. The fits of theoretically simulated absorption signals for the 6p resonance in xenon (lifetime = 21.1 fs) to this expression yield the correct decay constant for all the coupling mechanisms considered, properly recovering the time signature of twice the autoionization lifetime due to the coherent nature of the transient absorption experiment. To distinguish between these two coupling cases, the characteristic dependencies of the transient absorption signals on both the photon energy and time delay are investigated. Additional oscillations versus delay-time in the measured spectrum are shown and quantum beat analysis is used to pinpoint the major photon-coupling mechanism induced by the NIR pulse in the current xenon experiment: the NIR pulse resonantly couples the attosecond-probed state, 6p, to an intermediate 8s (at 22.563 eV), and this 8s state is also coupled to a neighboring state (at 20.808 eV).

Keywords: transient absorption, autoionization lifetime, quantum beat

(Some figures may appear in colour only in the online journal)

1. Introduction

As the technology to produce attosecond light pulses by the method of high harmonic generation advances, the use of attosecond pulses in time-resolved transient absorption spectroscopy has received considerable attention in the recent literature [1–13]. A major goal of these studies is to understand how the dynamics of photon coupling between the states of interest and other states of the target atom or molecule are manifested in the transient absorption spectrum.

Several previous investigations focused on electronically bound states of the target [6–9], while others considered the use of attosecond transient absorption as a probe of metastable (autoionizing) electronic states [10, 11]. Data are available for autoionizing excited states of xenon [11] and argon [12] investigated in recent experimental studies using transient absorption. The general experimental approach in these studies is to excite a state with an isolated extreme UV (XUV) attosecond pulse and to use a time-delayed near infrared (NIR) probe pulse to couple the system to neighboring states or continua, thus tracking the decay of the induced polarization versus time. In the case of xenon [11], we derived a simple expression that describes how the decay of a metastable state is manifested in the transient absorption spectrum and determined how the results are altered by tuning away from the line center in the time-resolved data.

Here we verify that this expression, which can be derived by using approximate models in several ways [10, 14], is more generally applicable to each of the specific coupling mechanisms of the NIR pulse. We explicitly consider cases in which a NIR probe pulse couples the metastable state to (1) a continuum and (2) a discrete state, resonantly or off-resonantly. We also study characteristics of the transient absorption signals by intense NIR pulses to explicitly distinguish between these two coupling cases. In addition, we show that features in a transient absorption spectrum, e.g. quantum beat oscillations of the signals versus time delay, can be used to obtain the locations of coupling states in the vicinity of the attosecond-probed state with opposite parity that do not appear as one photon transitions in the XUV absorption spectrum. These oscillations are a result of interferences between two quantum routes arising from coupling processes in the presence of the NIR pulse. Hence, the inverse of the oscillation period serves as a measure of the energy difference between the target state and a neighboring state of the same parity. Similar quantum beat effects have been studied theoretically [15] for XUV pump and strong NIR probe processes involving autoionizing states and experimentally for stable states below the ionization potential [16].

A basic point for this analysis is the essential way in which metastable states appear in attosecond transient absorption experiments based on a modification of the polarization of the medium, compared to other more direct pump–probe spectroscopic measurements. In the experiments under consideration, an XUV pulse first creates a polarization of the medium, i.e., a coherent superposition of the initial state with excited states of the target, here involving a metastable state that autoionizes during the time evolution of the polarization. A NIR pulse perturbs the polarization as a function of time delay [10–12]. As a result, the decaying part of the initially created coherence has a characteristic time of twice the lifetime of the metastable state. Observing this coherence differs from measurements of the population remaining in the metastable state, which has a characteristic time of just the lifetime [17, 18].

This paper is organized as follows. In section II, we review the theory involving the use of a two-state model and a

sudden approximation where the NIR field instantaneously annihilates the induced polarization to analytically derive a simple expression for the attosecond transient absorption spectrum as a function of photon energy and time-delay. In section III, we use numerical solutions of the time-dependent Schrödinger equation for few-level systems to investigate the general applicability of this simple expression for two NIR coupling cases. We also discuss the characteristic features in the absorption signals associated with each NIR coupling case at higher NIR intensities to identify the specific coupling mechanism for future experiments. Finally, in section IV, the appearance of oscillations in these spectra is explained in terms of quantum beats due to interference of two coupling routes that allows the inference of the locations of other resonances.

2. Two-level model for the transient absorption spectra

A two-level model leading to a simple description of the transient absorption spectra as a function of the time-delay and photon energy was introduced in [11], the detailed derivation of which is discussed in the following. If the time-dependent Hamiltonian can be expressed as $H = H_0 - \hat{\mu}\mathscr{E}(t)$ where H_0 is the field-free Hamiltonian, $\hat{\mu}$ is the dipole operator, and $\varepsilon(t)$ is the electric field of the applied laser pulse, the single-atom photon absorption spectrum can be expressed as [10, 19]

$$\tilde{S}(\omega) = 2\,\mathrm{Im}\left[\tilde{\mu}(\omega)\tilde{\mathscr{E}}^*(\omega)\right], \tag{1}$$

where $\tilde{\mu}(\omega)$ and $\tilde{\mathscr{E}}(\omega)$ are the Fourier transforms of the time-dependent induced dipole, $\mu(t) = \langle\Psi(t)|\hat{\mu}|\Psi(t)\rangle$, and the electric field, $\mathscr{E}(t)$, respectively.

Here, a two-level model is used to derive a basic formula to describe the transient absorption spectrum of a metastable state, which has been previously studied by others [10, 14] and by us [11]. In an attosecond transient absorption experiment, a sub-femtosecond XUV pulse excites the system from the ground state to a target resonance state, followed (or preceded) by a femtosecond intense NIR pulse at a time-delay t_{d}. After the initial excitation driven by the ultrashort XUV pulse and before the system is modified by the NIR pulse, it is assumed the total wave function of the target can be described by the ground state and the metastable state with explicit time dependences,

$$\Psi(t) = c_1 e^{-iE_1 t}\left|\psi_1\right\rangle + c_2 e^{-iE_2 t - \Gamma t/2}\left|\psi_2\right\rangle, \tag{2}$$

where E_1 and E_2 are the real energies of the ground and metastable states, respectively, and Γ is the width of the metastable state whose inverse is the lifetime. When the first XUV pulse is weak, c_1 is ≈ 1, and an approximation to the amplitude c_2 from first order perturbation theory can be made. In general, c_2 depends on the lifetime of the metastable state, but if the XUV pulse is short (sub-femtoseconds) compared to the lifetime (femtoseconds), it is expected that the XUV pulse

is complete before the target state decays significantly by autoionization. In the *absence* of the NIR pulse, the wave function defined in equation (2) can be used to evaluate the time-dependent induced dipole $\mu(t)$ as

$$\mu(t) = \left\langle \Psi(t) \left| \hat{\mu} \right| \Psi(t) \right\rangle$$
$$\approx c_2 \mu_{12} e^{-i\left(E_2 - \frac{i\Gamma}{2} - E_1\right)t} + \text{c.c.} , \qquad (3)$$

where $\mu_{12} = \left\langle \psi_1 \left| \hat{\mu} \right| \psi_2 \right\rangle$ is the transition dipole between the ground state and the resonance state.

In this model, a 'sudden approximation' is made: it is assumed that an infinitely short NIR pulse, which is applied at a time-delay t_d, is strong enough such that it extinguishes the population of the state ψ_2 instantly. Hence, the induced time-dependent dipole in equation (4) becomes

$$\mu(t) = \begin{cases} 0 & t < 0 \\ c_2 \mu_{12} e^{-i\left(E_2 - \frac{i\Gamma}{2} - E_1\right)t} + \text{c.c.} & 0 < t < t_d \\ 0 & t_d < t. \end{cases} \qquad (4)$$

By invoking the rotating wave approximation (RWA) for the XUV pulse, at a positive frequency ω, the Fourier transform of the induced dipole is

$$\tilde{\mu}(\omega) = \frac{1}{\sqrt{2\pi}} \int_0^{t_d} e^{i\omega t} c_2 \mu_{12} e^{-i\left(E_2 - \frac{i\Gamma}{2} - E_1\right)t} dt$$
$$= d_0 \frac{e^{-i\left(E_2 - \frac{i\Gamma}{2} - E_1 - \omega\right)t_d} - 1}{-i\left(E_2 - \frac{i\Gamma}{2} - E_1 - \omega\right)}, \qquad (5)$$

where $d_0 = c_2 \mu_{12}/\sqrt{2\pi}$ is a complex amplitude that depends on how the state was prepared by the preceding XUV pulse.

Defining a detuning variable $\Delta\omega = \omega - (E_2 - E_1)$, we can express the absorption spectrum as

$$\tilde{S}(\omega) = 2 \,\text{Im}\left[\tilde{\mu}(\omega) \tilde{\mathscr{E}}^*(\omega) \right] = A - B \exp\left(-\Gamma t_d/2\right)$$
$$\times \cos\left[\Delta\omega t_d + \phi\right], \qquad (6)$$

where A, B, and $\boldsymbol{\phi}$ depend on the laser parameters and the atomic properties but not on the time-delay t_d. Equation (6) shows the origin of the factor of two for the lifetime determination. The decaying part of the initially created coherence between the ground state and the excited state wave function has a characteristic time of twice the lifetime of the metastable state, which originates from equation (2). It was used in our previous study [11] and its applicability is further investigated here. It also describes the off-resonant behavior of the absorbance that leads to hyperbolic sideband structures. Similar expressions were also obtained in [10, 14] assuming the same sudden approximation. An intuitive physical picture of the origin of the $\cos\left[\Delta\omega t_d + \phi\right]$ behavior of the absorption spectrum can also be seen in this limit of a sudden annihilation by the NIR pulse of the oscillating and decaying dipole induced by the XUV pulse. In this limit the behavior is simply the ringing as a function of ω caused in $\tilde{\mu}(\omega)$ (the Gibbs phenomenon [20]) because it is the Fourier transform of a function that is sharply cut off at $t = t_d$.

3. Few-level model simulation results

Instead of relying on the sudden approximation, the current study aims at investigating the applicability of equation (6) to more general cases by assuming a NIR pulse with a finite temporal width and studying various photon couplings of the metastable state to neighboring states. We explicitly consider two cases in which a probe NIR pulse couples the metastable state to (1) a continuum and (2) a discrete state. Few-level models associated with these two NIR coupling cases are applied here to compute the transient absorption spectra as a function of the time-delay and photon energies, which are then compared to the expression in equation (6) to test its ability to describe the long time-delay behavior of the transient absorption signals for general cases. In these few-level models, instead of using a two-level system composed of only the ground and target resonance state, we explicitly include the NIR coupling terms between the target resonance state and a third state, continuum or discrete. More importantly, by varying the NIR pulse intensities used in the model simulations, we discuss the characteristic features of each NIR coupling case in both the frequency-resolved and delay-time-resolved absorption spectra. In addition, it is useful to understand some of the subtle features, e.g. an additional oscillation with time-delay appearing in the transient absorption signals of xenon [11], to extract information such as the energies of states coupled by the radiation fields and to pinpoint the primary photon-coupling mechanism for the experiments in xenon.

3.1. Few-level models: the discrete–continuum and discrete–discrete coupling cases

We start by describing the few-level models that we will use to compute the transient absorption signals associated with the discrete–continuum and discrete–discrete NIR coupling cases. We first study a case where the NIR pulse couples the metastable state to a continuum, for which we schematically show the energy levels and the couplings in figure 1(a). Here, an XUV pulse excites the system from the ground state, ψ_1, to a target resonance state, ψ_2; a NIR pulse couples the resonance state, ψ_2, to an ionization continuum, ψ_E. The total wave function, $\Psi(t)$, is expanded in terms of ψ_1, ψ_2, and ψ_E, which are coupled by an XUV pulse with a full-width-half-max (FWHM) of 470 attoseconds and a NIR pulse with a FWHM of 24 femtoseconds to match the current experiment [11]. The associated Hamiltonian can be expressed as

$$H(t) = H_0 - \mathscr{E}(t)$$
$$\times \left[\begin{array}{l} \left| \psi_1 \right\rangle \left\langle \psi_1 \left| \hat{\mu} \right| \psi_2 \right\rangle \left\langle \psi_2 \right| \\ + \int dE \left| \psi_E \right\rangle \left\langle \psi_E \left| \hat{\mu} \right| \psi_2 \right\rangle \left\langle \psi_2 \right| + \text{c.c.} \end{array} \right], \qquad (7)$$

where H_0 is the field-free Hamiltonian and $\mathscr{E}(t)$ is the combined electric field strength, and where the RWA is not assumed. The time-dependent Schrödinger equation for this three-state system is solved numerically to compute the population dynamics. The population dynamics of the
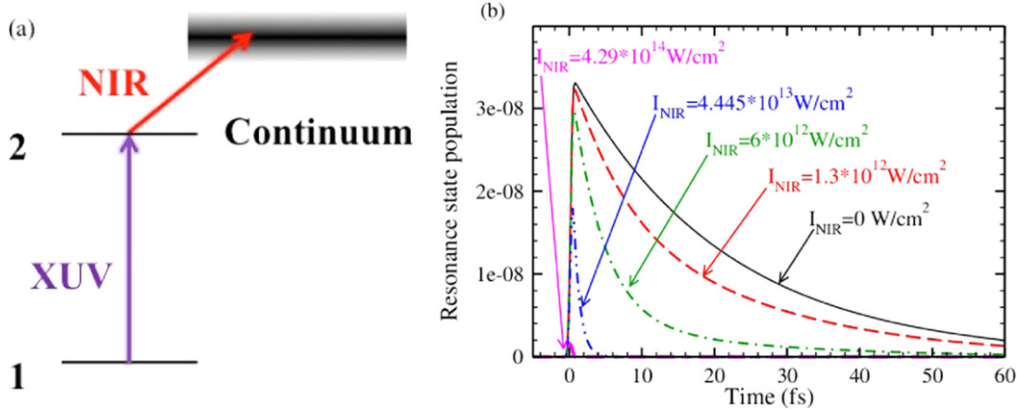
Figure 1. (a) Schematic diagram of energy levels and coupling schemes of a discrete–continuum case; (b) resonance-state population dynamics subject to various NIR laser intensities for the discrete–continuum coupling case with zero time delay.
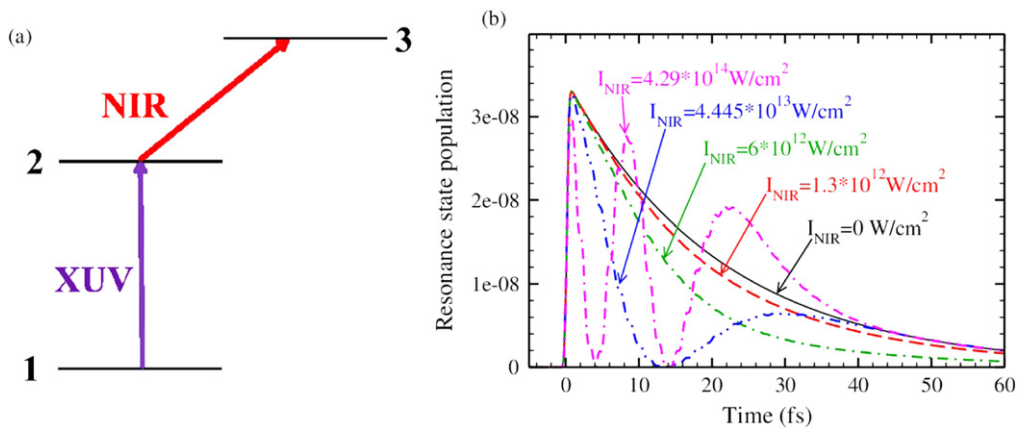

Figure 2. (a) Schematic diagram of energy levels and coupling schemes of a discrete–discrete case; (b) resonance-state population dynamics subject to various NIR laser intensities for the discrete–discrete coupling case with a zero time-delay.

target resonance state are shown in figure 1(b), for various NIR pulse intensities with zero time delay. Here, both autoionization and photoionization of the target resonance state occur when the NIR pulse is applied. At the highest NIR intensity used in the simulation, $I_{NIR} = 4.29 \times 10^{14}\,\mathrm{W\,cm^{-2}}$, the resonance-state is minimally populated because it is quickly ionized and depopulated by the intense NIR field.

Instead of directly ionizing the resonance state in the discrete–continuum case, the NIR pulse can alternatively couple the resonance state to another discrete state. Transitions between discrete states may lead to rich dynamics: Rabi cycles, Autler–Townes splittings [19], light induced states [21], and complex wave packet dynamics. Note that this discrete–discrete coupling scheme is similar to the case studied in [6, 9, 22] except for the fact that the discrete state here autoionizes and introduces additional features in the dynamics.

Next, consider resonant coupling of the attosecond-probed state to a discrete state. A schematic diagram of the energy levels and couplings associated with this discrete–discrete case is shown in figure 2(a). Here, in contrast to the discrete–continuum case, a NIR pulse couples the metastable state, ψ_2, resonantly to a third discrete state, ψ_3. The associated Hamiltonian can be expressed as,

$$H(t) = H_0 - \mathscr{E}(t)\Big[|\psi_1\rangle\langle\psi_1|\hat{\mu}|\psi_2\rangle\langle\psi_2| \\ + |\psi_3\rangle\langle\psi_3|\,\hat{\mu}\,|\psi_2\rangle\langle\psi_2| + \mathrm{c.c.}\Big]. \quad (8)$$

The time-dependent Schrödinger equation for this discrete–discrete case is numerically solved to calculate the population dynamics and the field-induced polarization. In figure 2(b), we show the simulated population dynamics of the attosecond-probed state with zero time delay for NIR pulses with different intensities. The NIR pulse drives population transfer between the attosecond-probed state and the third state, which can be understood as Rabi oscillations.

3.2. Similarities between the two NIR coupling cases: applicability of the simple expression and temporary broadening of the resonance line shape of the attosecond-probed state

We now discuss the similarities in the transient absorption signal between the two NIR coupling cases. To obtain the real-time tracking of the autoionizing resonance state for both the discrete–continuum case and the discrete–discrete NIR coupling case, the induced dipole is evaluated by
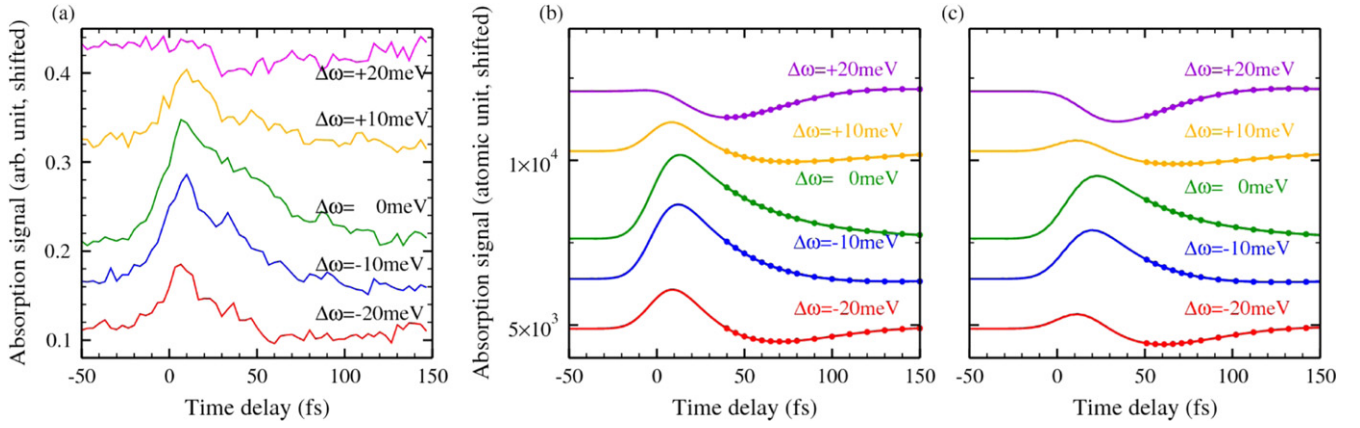
Figure 3. Absorption spectrum as a function of the time-delay at five photon energies: (a) experimental (reproduced from [11]), (b) discrete–continuum and (c) discrete–discrete case simulation (solid lines) fitted with equation (6) (filled circles) with $I_{NIR} = 1.3 \times 10^{12}$ W cm^{-2} and a NIR pulse temporal width of 24 fs.

$\mu(t) = \left\langle \Psi(t) \left| \hat{\mu} \right| \Psi(t) \right\rangle$ and used to compute the associated response function by $\tilde{S}(\omega)$ in equation (1). Considering the comparison, figure 3(a) (reproduced from [11]), figures 3(b), and (c) show the measured and simulated (for the discrete–continuum and resonant discrete–discrete NIR coupling cases) absorption signals as a function of time-delay and at five different detunings, $\Delta\omega$, near the xenon $5s5p^66p$ auto-ionizing resonance with $I_{NIR} = 1.3 \times 10^{12}$ W cm^{-2} and a NIR pulse temporal width of 24 fs. The experimentally measured spectra, shown in figure 3(a), agree qualitatively with equation (6) for long time delays. The fit to an exponential decay form of the resonance signal ($\Delta\omega = 0$) yields a decay constant of $1/(21.9 \pm 1.3$ fs), which corresponds to the expected lifetime of the 6p state obtained from the linewidth, 21.1 fs [23]. Note, equation [4] explicitly points out that the attosecond-induced polarization decays with a timescale of 42.2 fs, twice as much as the lifetime of the attosecond-probed state. If the NIR pulse duration were longer than the lifetime of the polarization, the extraction of the lifetime using equation [6] would have been less successful. The off-resonance behavior of the measured spectra in figure 3(a) also agrees qualitatively with the $\cos\left[\Delta\omega t_d + \phi\right]$ expression in equation (6), where the decaying signals oscillate with their detunings.

For the discrete–continuum and discrete–discrete coupling cases with the same pulse parameters as used in the experiment [11], the transient absorption signals are shown in figures 3(b) and (c), respectively. When the XUV and NIR pulse have a negligible temporal overlap for long time-delays, e.g. $t_d > 40$ fs, all the computed absorption signals at five detunings for both coupling cases can be fitted to equation (6) (filled circles), all leading to a fitted decay constant of $\Gamma_{fitted} = 1/(21.100 \pm 0.001$ fs). At higher NIR intensities, e.g. $I_{NIR} = 6 \times 10^{12}$ W cm^{-2}, 4.445×10^{13} W cm^{-2} and 4.29×10^{14} W cm^{-2}, the temporal behavior of $\tilde{S}(\Delta\omega, t_d)$ also agrees with equation (6) for both of the NIR coupling cases, only starting at longer time-delays. For $I_{NIR} = 6 \times 10^{12}$ W cm^{-2} and $I_{NIR} = 4.29 \times 10^{14}$ W cm^{-2}, when the XUV pulse is well in advance of the NIR pulse, the NIR pulse induces half of a

Rabi cycle and four Rabi cycles, respectively. Extracting the lifetime with an error smaller than 0.4 fs requires the fitting of the transient absorption signals to equation (6) beginning with t_d greater than 40 fs and 48 fs for $I_{NIR} = 6 \times 10^{12}$ W cm^{-2} and I_{NIR} 4.29×10^{14} W cm^{-2}, respectively. The disagreement at shorter time-delays for more intense NIR pulses is a result of an increase of the temporal overlap of the XUV and NIR pulse of the Gaussian pulse profiles. This difference will be extensively discussed in the next section. In addition to studying the case with the NIR field resonantly coupling the attosecond-probed state to a discrete state, we also investigate the off-resonance coupling case, where one could envision a Raman process connecting the ground state with the third state by absorbing an XUV photon and emitting a NIR photon via stimulated emission processes. The long-time behavior of the simulated spectra, where the NIR pulse is set to be off-resonant by 0.5 eV, again agrees well with the equation (6).

In spite of the additional features in the dynamics induced by the intense NIR field, e.g. multiple Rabi cycles in the discrete–discrete case, the long-time behavior of the absorption spectra agrees with equation (6) for both coupling cases and for all NIR intensities. This similarity in the long time behavior of the transient absorption signals can be understood by the fact that the NIR pulse plays the same role in both coupling cases: it modifies the population of the target resonance state and the associated induced polarization at a specific time-delay. Therefore, the similarity in the long time behavior of the simulated spectra between different NIR coupling cases indicates the general applicability of equation (6).

These two NIR coupling cases share another feature: the resonance line shapes can be temporarily broadened. An important observation in the current experiment is also that the resonance line shape is broadened transiently by the NIR pulse. At a specific time delay, the measured spectra are fitted with a Fano profile formula plus an additional background term to determine its width, as shown in figure 4 by the black circles with error bars. A 30% increase in the lineshape width is experimentally measured at $I_{NIR} = 1.3 \times 10^{12}$ W cm^{-2}. By studying the few-level models, we show in figure 4 the

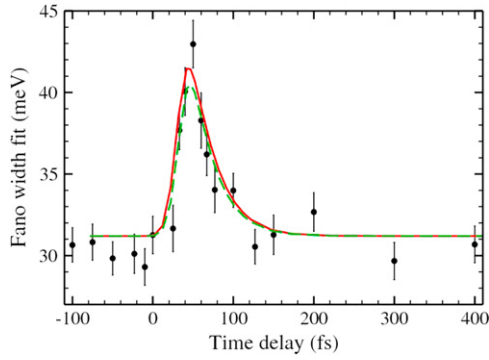J. Phys. B: At. Mol. Opt. Phys. **48** (2015) 125601

X Li *et al*

Figure 4. Extracted Fano widths as a function of time-delay from the experiment with error bars (black circles), a discrete–continuum case simulation (red solid line) and a discrete–discrete case simulation (green dashed line).

broadened width as a function of the time-delay for a discrete–continuum case (red solid line) or a discrete–discrete case (green dashed line), where the same temporary broadening of the resonance is observed as seen in the experiment. Note that the two curves corresponding to the theoretical simulations are shifted to the right (longer time-delay) by 20 fs to match the maximal broadening occurring at a time-delay of 45 fs as measured in the experiment. Note direct measurement of the absolute time-delay is difficult and thus the absolute zero time-delay in figure 4 is unknown for the current experiment. The agreement of the time-dependent Fano width results as displayed in figure 4 is used in this study to calibrate the model parameters with the NIR laser intensity set at 1.3×10^{12} W cm^{-2} as used in the experiment [11]. The same model parameters are also used in the simulations for the following discussions where the NIR laser intensities are varied in both of the coupling cases, discrete–continuum or discrete–discrete.

3.3. Difference between the two NIR coupling cases in the frequency resolved and delay-time-resolved absorption spectra

Despite the similarities in the transient absorption signals between the two coupling cases, there are features that one could in principle observe in the experiment to identify the specific coupling mechanism. We investigate the change of resonance line shape in the absorption spectrum as a function of the NIR intensity with zero time-delay, where the XUV and NIR pulses have a maximal temporal overlap. For the discrete–continuum case, as the NIR intensity increases, the Fano line shape disappears and the spectrum approaches that of a flat line resembling the direct photoionization background, as shown in figure 5(a). This change of line shapes is reasonable: When the XUV and NIR pulses have a significant temporal overlap, the intense NIR field quickly ionizes the metastable resonance state before this state can autoionize. Hence, this additional ionization process induced by the NIR field eventually supersedes the field-free autoionization pathway and hence the associated quantum interference leading to the Fano shape.

In contrast, for the discrete–discrete case, NIR pulses with various intensities modify the resonance line shapes differently. In figure 5(b), we show the simulated spectra using four NIR intensities. If the dressing field (NIR) were to have a long pulse duration, one would observe Autler–Townes splittings, in which a single resonance splits into two resonances separated by twice the maximal Rabi frequency. However, for the short dressing (NIR) pulses used in the current study, one does not observe a clear splitting. Instead, figure 5(b) shows that the static resonance line shape (solid black lines) is modified by strong photon-couplings of the resonance state to a third state. For the most intense pulse applied in the theoretical simulation, $I_{NIR} = 4.29 \times 10^{14}$ W cm^{-2}, the maximal Rabi frequency is $\Omega_{NIR} = 0.254$ eV, which is defined as $\Omega_{NIR} = \mathscr{E}_{NIR}\mu_{23}/2$, where $\mathscr{E}_{NIR}$ is the maximal electric field strength of the NIR field and μ_{23} is the transition dipole moment between the resonance state and the third state. In this case, pairs of enhanced absorption features, separated by 0.11 eV, and pairs of suppressed absorption features, separated by 0.38 eV, are observed. However, due to the limit of the available experimental NIR intensities, the substantial changes in the resonance line shape at $I_{NIR} = 4.445 \times 10^{13}$ W cm^{-2} and 4.29×10^{14} W cm^{-2} as predicted by theory are not accessible in the current experiment. A minimum NIR intensity of 2×10^{13} W cm^{-2} is needed to distinguish between NIR coupling cases. For the same reason, multiple absorption peaks separated by the NIR central frequency in the energy domain predicted by [22] are also not explored here. In addition, a transition from a Fano profile to a Lorentzian shape as seen in [5] is not observed.

In addition to the difference in how the resonance line shapes are modified by the NIR field, as the NIR intensity increases, the time-delay dependence of the transient absorption spectra also differs for the two coupling cases. For the discrete–continuum case as shown in figure 6(a), as more intense NIR fields are applied, little additional structure is observed where the XUV and NIR pulses overlap, -40 fs $< t_d < +40$ fs. However, for the discrete–discrete case, when the XUV and NIR pulses overlap, more intense NIR fields lead to bigger modifications of the absorption signals. Here, as shown in figure 6(b) for a NIR pulse with $I_{NIR} = 4.29 \times 10^{14}$ W cm^{-2}, the temporal difference between the two maxima is approximately 18 fs, the inverse of which yields an oscillating frequency of 0.23 eV. This oscillating frequency is very close to the maximal Rabi frequency $\Omega_{NIR} = 0.254$ eV associated with discrete–discrete coupling that would be induced by this NIR pulse; similar effects were also predicted in [9].

4. Quantum beats from coupling of neighboring resonance states

Here we show that subtle features in a transient absorption spectrum, e.g. oscillations of the signals versus time delay, can be useful for determining the locations of the states in the
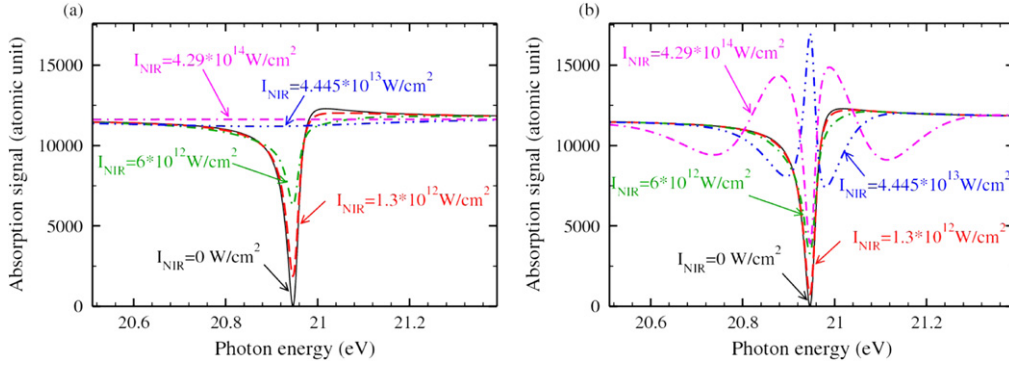
Figure 5. Photon energy dependence of the transient absorption spectra at various NIR intensities near the 6p resonance for (a) the discrete–continuum and (b) the discrete–discrete coupling schemes.
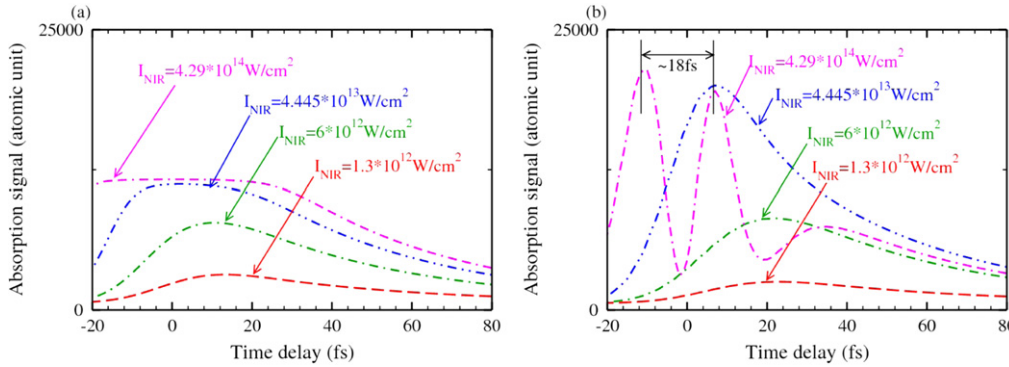

Figure 6. Time-delay dependence of the transient absorption spectra at various NIR intensities at the 6p resonance for (a) the discrete–continuum and (b) the discrete–discrete coupling schemes.

vicinity of the attosecond-probed state. In addition, by studying the roles of these states in the associated dynamics, we find these oscillation features useful for identifying the primary photon coupling mechanism induced by the NIR field in the current experiment as to whether the attosecond-probed state is coupled to discrete states resonantly or off-resonantly, or to continuum states.

4.1. Theory

In the measured absorption spectrum, an additional oscillation versus time-delay is observed for autoionizing states in xenon [11]; a similar result has been reported for stable states in neon [16]. At the odd-parity 6p resonance in Xe, the observed signals oscillate with a period of approximately 29 fs as shown by the dots in figure 7(a). In this study, such an oscillation is attributed to the existence of a neighboring resonance, which is also optically coupled to the ground state by the XUV pulse and to the 6p state via a Raman process by the NIR pulse, as depicted schematically in figure 7(b). This oscillation is a result of interferences between two quantum routes arising from multi-photon processes in the presence of the intense NIR field. The first route involves an XUV photon being absorbed that excites the system from the ground state to the attosecond-probed state. The second route depicts a process where the system absorbs a different XUV photon to the neighboring state, absorbs and emits NIR photons and reaches the attosecond-probed state again. These two

quantum routes lead to interference patterns in the created polarization as a function of time-delay. Hence, in the transient absorption spectrum, a beating pattern can be observed with a period determined by the inverse of the energy difference between these two states initially excited by the XUV pulse. This quantum beat phenomenon in the transient absorption spectrum is similar to a wave packet interferometry experiment [24] where an initial pulse prepares a wave packet and a subsequent pulse probes how coherence has evolved within the wave packet during the time delay between the two pulses.

To investigate the quantum beat phenomenon in transient absorptions, we construct a four-level model to describe the associated physics as shown in figure 7(b). The associated Hamiltonian can be expressed as

$$
\begin{aligned}
H(t) = H_0 - \mathscr{E}(t) \Big[& \big| \psi_1 \big\rangle \big\langle \psi_1 \big| \hat{\mu} \big| \psi_2 \big\rangle \big\langle \psi_2 \big| \\
+ & \big| \psi_3 \big\rangle \big\langle \psi_3 \big| \hat{\mu} \big| \psi_2 \big\rangle \big\langle \psi_2 \big| + \text{c.c.} \Big] \\
- \mathscr{E}(t)^* \Big[& \big| \psi_1 \big\rangle \big\langle \psi_1 \big| \hat{\mu} \big| \psi_{2'} \big\rangle \big\langle \psi_{2'} \big| \\
+ & \big| \psi_3 \big\rangle \big\langle \psi_3 \big| \hat{\mu} \big| \psi_{2'} \big\rangle \big\langle \psi_{2'} \big| + \text{c.c.} \Big].
\end{aligned}
\tag{9}
$$

We denote this photon-coupling scheme here as a 'double-resonance case'. Similar to the derivation of equation (6), an analytical expression of the transient absorption signals at the attosecond-probed resonance can be obtained by
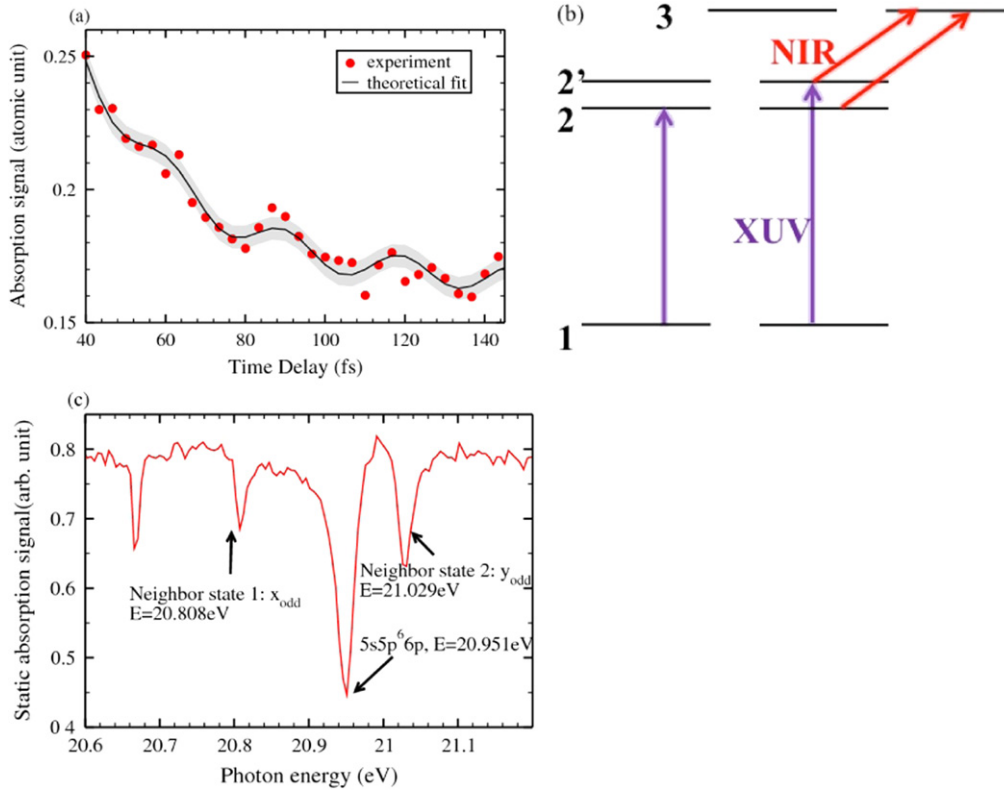
Figure 7. (a) Experimentally measured transient absorption signals at the 6p resonance (dots) fitted to the double-resonance formula in equation (7) (solid line), (b) energy levels and coupling schemes of a double-resonance case, and (c) the static absorption (NIR free) spectrum near the 6p target resonance state.

assuming the 'sudden approximation' when the NIR pulse is infinitely short

$$\tilde{S}'\left(\Delta\omega, t_{d}\right) = A - B\mathrm{e}^{-\frac{\Gamma t_{d}}{2}} - C\mathrm{e}^{-\frac{\Gamma' t_{d}}{2}}\cos\left[2\pi t_{d}/\tau + \phi'\right],$$
(10)

where Γ' is the energy width of this neighboring state of the same parity and τ is the oscillation period (the inverse of the energy difference between the two odd-parity states). Compared to equation (6), an additional term is present in equation (10), which corresponds to the contribution from this neighboring state to the absorption signals at the resonance of the attosecond-probed state. This expression is later used to fit the experimentally measured transient absorption spectra to extract the oscillating period as shown in figure 7(a) and deduce the energy difference between the two odd-parity states.

To demonstrate such an effect more rigorously, the time-dependent Schrödinger equation for this four-level model is numerically solved without using the 'sudden approximation' that was used to derive equation (10). From time-independent spectra measured in [23, 25] and our static absorption spectrum [11], the neighboring state 1 as shown in figure 7(c) is known to be 0.143 eV below the 6p state. This neighboring state is denoted in this study as x_{odd} because of its odd parity nature and as yet unknown electronic structure. This x_{odd} state is used as the state 2' in the four-level model because it is 0.143 eV away from the target-resonance state, 6p, where the
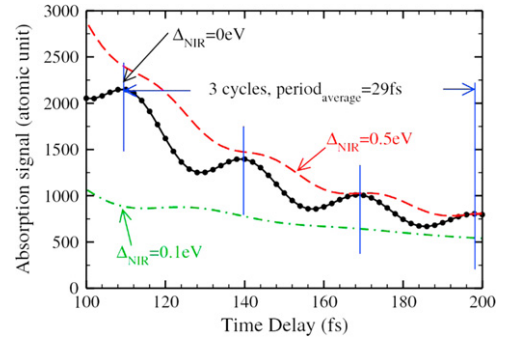

Figure 8. Simulated absorption signals for the double-resonance case at the 6p resonance for $\Delta_{NIR} = 0$ eV (black solid line), 0.1 eV (red dashed line), and 0.5 eV (green dot-dash line).

inverse of the energy difference is approximately 29 fs as indicated from our experiment. For simplicity, we don't include the effect from another neighboring state located at 0.087 eV above the 6p resonance state, denoted by y_{odd}. The lifetime of the x_{odd} state is assumed to be much longer than 6p. The numerically simulated absorption signals at the 6p resonance (black circles) are shown in figure 8, where we choose the NIR detuning $\Delta_{NIR} = E_{3} - (E_{6p} + \hbar\omega_{NIR}) = 0$ and a pulse temporal width of 24 fs. The simulated results (black circles) agree very well to the quantum-beat expression in equation (10) (black solid line) as expected.

We can also extract information about the location of the even-parity intermediate that must be present to couple the
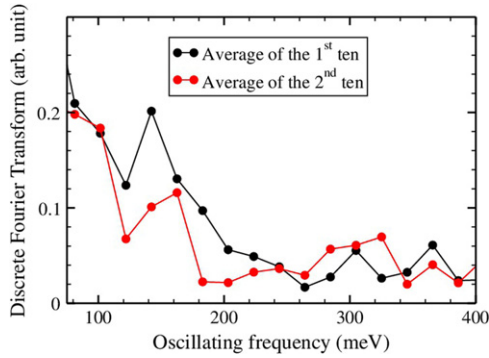
J. Phys. B: At. Mol. Opt. Phys. **48** (2015) 125601

X Li *et al*

Figure 9. Fourier transform of the measured absorption signals over the time-delay at the 6p resonance ($\Delta\omega = 0$) for averaged spectra over ten measurements.

odd-parity 6p and x_{odd} states. Setting the pulse temporal width as $FWHM_{NIR} = 24\,fs$ and examining the simulated spectra using three NIR detunings, $\Delta_{NIR} = 0\,eV$ (black solid line), 0.1 eV (red dashed line), and 0.5 eV (green dot-dash line) shown in figure 8, it can be seen that larger NIR detunings lead to smaller oscillation amplitudes. This finding strongly suggests that, for the oscillation to be visible in the absorption signal, the NIR detuning is required to be small and thus this coupling intermediate should be in the vicinity of $E_{6p} + \hbar\omega_{NIR} = 22.51\,eV$. This even-parity intermediate is thus identified as the $5s5p^6 8s$ state, measured previously at 22.563 eV by electron impact [26]. Even though this 8s state is dark from the ground state via a one-photon process, this analysis provides a way to both identify its parity and infer its location.

4.2. Experiment

The fit of the measured signals at the 6p resonance (dots) in figure 3(a) to the quantum beat expression of equation (10) (solid line) leads to an extracted oscillating period of $\tau = 29 \pm 1\,fs$, as shown in figure 9(a) with a shaded boundary to represent the root-mean-square error. A nonlinear optimization method that is based on the Levenberg–Marquardt algorithm [27] is applied with initial guesses of this oscillation period in the range of 20 to 60 fs. The inverse of this extracted oscillating period, $2\pi\hbar/(29 \pm 1\,fs) = 0.143 \pm 0.005\,eV$, agrees with the measured energy difference in the static spectra, 0.143 eV, between this neighboring odd-parity state x_{odd} and the 6p state [11, 23, 25]. To investigate whether the oscillation period of 29 fs is due to random error, we plot the Fourier transform of the absorption signal over the time-delay at the 6p resonance for averaged spectra over ten measurements in figure 9, where the signal near the oscillating frequency of 0.143 eV is evident. We suggest that the persistent signal in the Fourier transform over the time-delay at this particular frequency of 0.143 eV indicates that this oscillation versus time-delay is not likely due to random noise. Note that a slower oscillation of the absorption signals near the 6p resonance versus time delay is also observed due to the neighboring state 2 in figure 7(c) that is located at

0.087 eV away from the 6p state, as shown in figure 7(c). This slower oscillation is obvious over the noise.

The quantum beat analysis of the oscillation thus provides a way to identify the photon coupling mechanism in this experiment: the NIR field resonantly couples the attosecond-probed state, 6p, to a discrete state, 8s. As shown in figure 8, if the 6p and x_{odd} states were instead coupled primarily off-resonantly through discrete states these oscillations related to their energy separation would not appear in the transient absorption spectrum. By performing a similar calculation, we find that, if the 6p and x_{odd} states were instead coupled primarily through continuum states, the absorption signals near the 6p resonance would not be different from that in figure 3(b) and would show much weaker oscillations. Similar quantum beats between bound states have been observed in a recent experiment of neon atoms with attosecond laser pulses [16]. Vibrational quantum beats between decaying Rydberg states have also been previously measured with transient absorption experiments with picosecond lasers [28, 29].

5. Conclusion

In summary, we have analyzed attosecond transient absorption spectra near the energies of autoionizing states in terms of the photon coupling to other states. A simple expression, which was used to describe how the decay of a metastable state at long time-delays was manifested in a recent transient absorption measurement [11], is more general and can be used in cases involving the resonant or nonresonant coupling of the attosecond-probed autoionizing state to either continua or discrete states by a time delayed NIR pulse. The fits of the theoretically simulated absorption signals at the 6p resonance (lifetime = 21.1 fs) to this simple expression yield the correct decaying constant for all three photon coupling mechanisms considered, properly recovering the time signature of twice the autoionization lifetime due to the coherent nature of the transient absorption experiment. By studying the characteristic dependence of the absorption signals on both the photon energy and time delay at higher NIR intensities than were used in the current experiment, we explicitly distinguish between the two coupling cases, and suggest a way to identify the NIR coupling mechanism for future transient absorption experiments. We find that a minimum NIR intensity of $2 \times 10^{13}\,W\,cm^{-2}$ is needed to distinguish between NIR coupling cases in Xe. An additional fast oscillation with time delay in the measured spectrum at the odd-parity 6p resonance is shown. More importantly, a quantum beat analysis is used to pinpoint the major photon-coupling mechanism induced by the NIR pulse in the current xenon experiment: the NIR pulse resonantly couples the attosecond-probed state, 6p, to an intermediate 8s (at 22.563 eV), which is also coupled to a neighboring state, x_{odd} (0.143 eV below the 6p state).

For all the theoretical investigations involved in this study, the carrier envelope phase (CEP) of the NIR field is first taken to be zero. Additional studies of the CEP effect for three couplings mechanisms associated with coupling the 6p state to a continuum, to a discrete state resonantly, and to a

discrete state off-resonantly all show that the absorption spectrum has little CEP dependence. This behavior is probably due to the limited intensity in this simulation and a relatively long pulse-duration (FWHM$_{NIR}$ = 24 fs) compared to the optical period (∼2.7 fs) of the NIR field. Therefore, the conclusion drawn from this study on the general applicability of equation (6) to describe the long time behavior of the transient absorption signals can be applied to both CEP stabilized pulses or pulses integrated over random CEP values. However, if the pulse duration of the applied NIR pulse is much shorter and with a much larger intensity such that transient absorptions become CEP-dependent, the measured transient absorption spectrum becomes integrated over CEP values, a situation requiring a modification of the present treatment. This analysis of attosecond transient absorption measurements of the lifetimes of metastable states is currently being extended to more complex cases.

Acknowledgments

References

[1] See, e.g. Krausz F and Ivanov M 2009 *Rev. Mod. Phys.* **81** 163
[2] Goulielmakis E *et al* 2010 *Nature* **466** 739
[3] Schultze M, Bothschafter E M, Sommer A, Holzner S, Schweinberger W, Fiess M, Hofstetter M, Kienberger R, Apalkov V and Yakovlev V S 2013 *Nature* **493** 75
[4] Chini M, Wang X W, Cheng Y, Wu Y and Zhao D 2013 *Sci. Rep.* **3** 1105
[5] Ott C, Kaldun A, Raith P, Meyer K, Laux M, Evers J, Keitel C H, Greene C H and Pfeifer T 2013 *Science* **340** 716
[6] Wu M, Chen S, Gaarde M B and Schafer K J 2013 *Phys. Rev. A* **88** 043416
[7] Santra R, Yakovlev V S, Pfeifer T and Loh Z-H 2011 *Phys. Rev. A* **83** 033405
[8] Chen S *et al* 2012 *Phys. Rev. A* **86** 063408
[9] Chen S, Wu M, Gaarde M B and Schafer K J 2013 *Phys. Rev. A* **87** 033408
[10] Chu W C and Lin C D 2013 *Phys. Rev. A* **87** 013415
[11] Bernhardt B, Beck A R, Li X, Warrick E, Bell M J, Haxton D J, McCurdy C W, Neumark D M and Leone S R 2014 *Phys. Rev. A* **89** 023408
[12] Wang H, Chini M, Chen S, Zhang C-H, He F, Cheng Y, Wu Y, Thumm U and Chang Z 2010 *Phys. Rev. Lett.* **105** 143002
[13] Schultze M *et al* 2014 *Science* **346** 1348
[14] Pfeiffer A N, Bell M J, Beck A R, Mashiko H, Neumark D M and Leone S R 2013 *Phys. Rev. A* **88** 051402
[15] Zhao Z X and Lin C D 2005 *Phys. Rev. A* **71** 060702
[16] Beck A R, Bernhardt B, Warrick E R, Wu M, Chen S, Gaarde M B, Schafer K J, Neumark D M and Leone S R 2014 *New J. Phys.* **16** 113016
[17] Drescher M, Hentschel M, Kienberger R, Uiberacker M, Yakovlev V, Scrinzi A, Westerwalbesloh T, Kleineberg U, Heinzmann U and Krausz F 2002 *Nature* **419** 803
[18] Gilbertson S, Chini M, Feng X, Khan S, Wu Y and Chang Z 2010 *Phys. Rev. Lett.* **105** 263003
[19] Gaarde M B, Buth C, Tate J T and Schafer K J 2011 *Phys. Rev. A* **83** 013419
[20] Gibbs J W 1898 *Nature* **59** 200
[21] Bell M J, Beck A R, Mashiko H, Neumark D M and Leone S R 2013 *J. Mod. Opt.* **60** 1506
[22] Pfeiffer A N and Leone S R 2012 *Phys. Rev. A* **85** 053422
[23] Ederer D L 1971 *Phys. Rev. A* **4** 2263
[24] See, e.g. Ohmori K 2009 *Annu. Rev. Phys. Chem.* **60** 487
[25] Cubric D, Thompson D B, Cooper D R, King G C and Read F H 1997 *J. Phys. B: At. Mol. Opt. Phys.* **30** L857
[26] Yuan Z-S, Sakai Y, Umeda N, Fujita Y, Takayanagi T, Yamada C, Nakamura N, Ohtani S, Zhu L-F and Xu K Z 2006 *J. Phys. B: At. Mol. Opt. Phys.* **39** 5097
[27] Mor J J, Sorensen D C, Hillstrom K E and Garbow B S 1984 *Sources and Development of Mathematical Software* ed W J Cowell (Englewood Cliffs, NJ: Prentice-Hall) pp 88–111
[28] Knappenberger K L Jr, Lerch E W, Wen P and Leone S R 2006 *J. Chem. Phys.* **125** 174314
[29] Dai X, Torres E A, Lerch E W, Wilson D J and Leone S R 2005 *Chem. Phys. Lett.* **402** 126